AMERICAN SOCIETY FOR MICROBIOLOGY | Journal of Virology®

GENOME REPLICATION AND REGULATION OF VIRAL GENE EXPRESSION

Interplay between the Poly(A) Tail, Poly(A)-Binding Protein, and Coronavirus Nucleocapsid Protein Regulates Gene Expression of Coronavirus and the Host Cell

Tsung-Lin Tsai,[a] Ching-Houng Lin,[a] Chao-Nan Lin,[b] Chen-Yu Lo,[a] Hung-Yi Wu[a]

[a]Graduate Institute of Veterinary Pathobiology, College of Veterinary Medicine, National Chung Hsing University, Taichung, Taiwan

[b]Department of Veterinary Medicine, National Pingtung University of Science and Technology, Neipu, Pingtung, Taiwan

ABSTRACT In the present study, we investigated the roles of interactions among the poly(A) tail, coronavirus nucleocapsid (N) protein, and poly(A)-binding protein (PABP) in the regulation of coronavirus gene expression. Through dissociation constant (K_d) comparison, we found that the coronavirus N protein can bind to the poly(A) tail with high affinity, establishing N protein as a PABP. A subsequent analysis with UV cross-linking and immunoprecipitation revealed that the N protein is able to bind to the poly(A) tail in infected cells. Further examination demonstrated that poly(A) tail binding by the N protein negatively regulates translation of coronaviral RNA and host mRNA both *in vitro* and in cells. Although the N protein can interact with PABP and eukaryotic initiation factor 4G (eIF4G), the poor interaction efficiency between the poly(A)-bound N protein and eIF4E may explain the observed decreased translation efficiency. In addition to interaction with translation factor eIF4G, the N protein is able to interact with coronavirus nonstructural protein 9 (nsp9), a replicase protein required for replication. The study demonstrates interactions among the poly(A) tail, N protein, and PABP both *in vitro* and in infected cells. Of the interactions, binding of the poly(A) tail to N protein decreases the interaction efficiency between the poly(A) tail and eIF4E, leading to translation inhibition. The poly(A)-dependent translation inhibition by N protein has not been previously demonstrated and thus extends our understanding of coronavirus gene expression.

IMPORTANCE Gene expression in coronavirus is a complicated and dynamic process. In this study, we demonstrated that coronavirus N protein is able to bind to the poly(A) tail with high affinity, establishing N protein as a PABP. We also show how the interplay between coronavirus 3′ poly(A) tail, PABP, and N protein regulates gene expression of the coronavirus and host cell. Of the interactions, poly(A) tail binding by the N protein negatively regulates translation, and to our knowledge, this inhibition of translation by binding of the N protein to poly(A) tail has not been previously studied. Accordingly, the study provides fundamental molecular details regarding coronavirus infection and expands our knowledge of coronavirus gene expression.

KEYWORDS RNA synthesis, coronavirus, gene expression, nucleocapsid protein, poly(A) tail, poly(A)-binding protein, replication, translation

Members of the family *Coronaviridae*, order *Nidovirales*, are single-stranded, positive-sense RNA viruses with the largest known viral RNA genome, 26 to 32 kb (1–3). The coronavirus genome consists of a 5′ cap, a 5′ untranslated region (UTR), open reading frames (ORFs), a 3′ UTR, and a 3′ poly(A) tail. The 5′ two-thirds of the genome consists of two ORFs (ORF 1a and ORF 1b) that encode 16 nonstructural proteins (nsps)

Received 6 July 2018 **Accepted** 30 August 2018

Accepted manuscript posted online 12 September 2018

Citation Tsai T-L, Lin C-H, Lin C-N, Lo C-Y, Wu H-Y. 2018. Interplay between the poly(A) tail, poly(A)-binding protein, and coronavirus nucleocapsid protein regulates gene expression of coronavirus and the host cell. J Virol 92:e01162-18. https://doi.org/10.1128/JVI.01162-18.

Editor Anne E. Simon, University of Maryland, College Park

Address correspondence to Hung-Yi Wu, hwu2@dragon.nchu.edu.tw.

with replicase activity. The other one-third of the genome largely consists of genes encoding structural proteins (3). During coronavirus infection, in addition to the replication of genomic RNA, coronaviruses synthesize a 3′-coterminal nested set of subgenomic mRNAs (sgmRNAs) from which the 5′-most ORF is translated (3).

The nucleocapsid (N) protein of coronaviruses, with a molecular weight of 50 to 55 kDa, is abundantly produced during infection. It has been shown that N protein binds to different sites of the coronaviral RNA genome with various binding affinities (4–7). Furthermore, the binding of N protein to coronaviral RNA is more efficient than to noncoronaviral RNA (6); however, it has yet to be examined whether coronavirus N protein is able to bind to the poly(A) tail. In addition to its structural role in the formation of ribonucleoprotein, N protein has been shown to interact with coronaviral replicase proteins, including nsp2, nsp3, nsp5, nsp8, nsp12, and nsp13 (8–14), and is required for efficient replication (15–19). Coronavirus nsp9 is a replicase protein and has been shown to be associated with polymerase nsp12 (20), essential for replication (21) and involved in the initiation of negative-strand RNA synthesis (22); however, whether nsp9 is able to interact with N protein remains unknown.

Poly(A)-binding protein (PABP), a 70-kDa cellular protein, is a ubiquitous cytosolic protein (23, 24). The binding of PABP to mRNA poly(A) tails is followed by interactions with eukaryotic initiation factor (eIF4G) and other translation factors, including eIF4E, to constitute a translation initiation complex, which mediates cellular mRNA circularization and enhances cap-dependent translation by facilitating ribosome recycling (24–26). The positive-strand coronavirus genome contains an m7GpppN-cap structure at the 5′ end and a poly(A) tail at the 3′ end, which are presumed to initiate translation in a way similar to that for cellular mRNA (3).

During coronavirus infection, the positive-strand genome functions as a template for both the synthesis of viral proteins and replication of the genome. Accordingly, a conflict may occur between the translation and replication machineries, as the ribosomes are moving along the viral RNA in the 5′-to-3′ direction and the viral RNA polymerase is moving in the opposite direction (3′ to 5′). Therefore, a balance between these two processes must exist to enable efficient viral gene expression. In poliovirus, it has been demonstrated that the 5′-terminal cloverleaf on the viral genome functions as a regulator to control the use of the genome for translation or replication (27, 28). Binding of poly(C)-binding protein (PCBP) to this RNA structure facilitates viral translation (internal ribosome entry site [IRES]-dependent translation), whereas interaction of the viral protein 3CD with this RNA structure represses translation and enhances replication. However, for coronaviruses, which employ a translation mechanism (cap-dependent translation) different from that of poliovirus, the strategy for coordinating the use of the positive-sense genome for translation or replication has yet to be determined.

Here we show that the bovine coronavirus (BCoV) N protein can bind to a poly(A) tail with high affinity. We also demonstrate that poly(A) tail binding by the N protein negatively regulates translation of coronaviral RNA and host mRNA. Finally, we demonstrate interactions among the poly(A) tail, PABP, and N followed by interactions with eIF4G, eIF4E, and nsp9. Based on these data, we propose a model explaining how these interactions regulate gene expression during coronavirus infection.

RESULTS

Coronavirus N protein binds to poly(A) tail with high affinity. It has been shown that N protein binds to different sites of the coronaviral RNA genome with various binding affinities (4–7); however, it has yet to be examined whether coronavirus N protein is able to bind to the poly(A) tail, a common structure in coronavirus genome, subgenomic mRNAs, and cellular mRNA. For this, we first tested whether *Escherichia coli*-expressed N protein (~65 kDa) (Fig. 1B) binds to the ^{32}P-labeled poly(A) tail using electrophoretic mobility shift assay (EMSA). As shown in Fig. 1C, N protein bound to the ^{32}P-labeled 65-nucleotide (nt) poly(A) tail (lane 2). In addition, a nonradiolabeled 65-nt poly(A) tail was able to compete for this binding by N protein in a dose-dependent

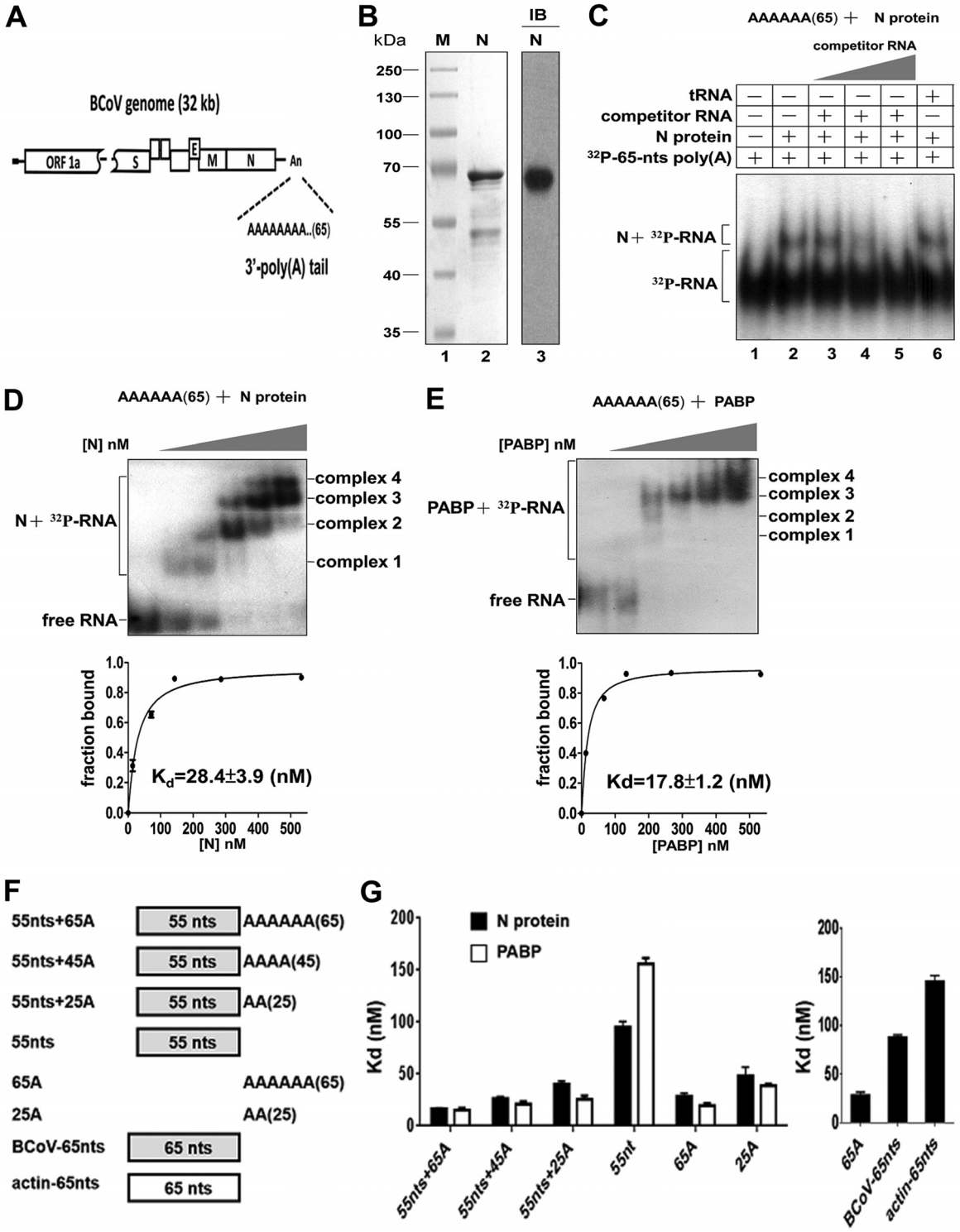

FIG 1 Coronavirus N protein binds to poly(A) tail with high affinity. (A) Schematic diagram showing the position of the poly(A) tail in the coronavirus genome. (B) *E. coli*-expressed coronavirus N protein (~65 kDa) stained with Coomassie blue (left) or analyzed by immunoblotting (IB; right). (C) EMSA showing the binding specificity of the 65-nt poly(A) tail with N protein. Unlabeled competitor was at 1-, 10-, and 100-fold excesses, and nonspecific yeast tRNA (0.1 mg/ml) was also used. (D and E) (Top) EMSA in binding experiments using a fixed concentration of ^{32}P-labeled 65-nt poly(A) tail with increasing amounts (0, 14, 71, 143, 286, and 533 nM) of N protein (D) or PABP (E). Complexes 1 to 4 in panel D were predicted to consist of 1 to 4 N proteins, respectively, and the ^{32}P-labeled 65-nt poly(A) tail, while complexes 1 to 4 in panel E were predicted to consist of 1 to 4 PABPs, respectively, and the ^{32}P-labeled 65-nt poly(A) tail. (Bottom) A plot of a fraction of bound RNA against the protein concentration is presented for the gel in the top portion and fits the Hill equation for K_d determination. (F) RNA probes used for determination of the binding affinity with N protein and PABP. (G) K_d values of RNA probes illustrated in panel F with N protein and PABP. Values in panels D, E, and G represent means ± SD from three independent experiments.

manner (lanes 3 to 5). Conversely, similar results were not found for the binding between N protein and yeast tRNA (lanes 6) or between glutathione *S*-transferase (GST) and the ^{32}P-labeled 65-nt poly(A) tail (data not shown). The data suggest that coronavirus N protein is able to bind to the poly(A) tail.

As it is well characterized that PABP binds to poly(A) tails with high affinity, we postulated that the potential significance of the poly(A)-binding activity of N protein may be further emphasized if its binding affinity is similar to that of PABP. For this reason, increasing concentrations of N protein and PABP were separately incubated with the ^{32}P-labeled 65-nt poly(A) tail and then analyzed by EMSA. The percentage of bound RNA was then used to derive the dissociation constant (K_d) using the Hill equation; the K_ds were calculated to be 28.4 $\pm$ 3.9 and 17.8 $\pm$ 1.2 nM for N protein and PABP (Fig. 1D and E), respectively, suggesting that N protein and PABP have similar binding affinities for the 65-nt poly(A) tail. Because the C-terminal domain (CTD) of N protein is mainly involved in oligomerization (29, 30) and the CTD of PABP has also been reported to possess homodimerization activity (31), the multiple complexes shown in Fig. 1D and E resulting from such protein-protein interaction are not unexpected.

To further characterize the poly(A)-binding activity of N protein, RNA probes with various sequences were synthesized (Fig. 1F). The same RNA probes were also examined for the ability to interact with PABP. The K_d for N protein and PABP with RNA probes containing the BCoV 3′-terminal 55 nt and poly(A) tails of decreasing lengths (55 nt + 65 A's [65A], 55 nt + 45A, 55 nt + 25A, or 55 nt) increased (Fig. 1G, left graph), suggesting that the length of the poly(A) tail is the main factor for increasing the binding efficiency of N protein and PABP to the RNA probes. In addition, the K_d for N protein and PABP with the 25-nt poly(A) tail was higher than that with the 65-nt poly(A) tail (Fig. 1G, left graph), further suggesting that N protein is a poly(A)-binding protein. Finally, as shown in Fig. 1G (right graph), the K_d for N protein and these non-poly(A) sequences containing various types of nucleotides (sequences designated BCoV-65nts and β-actin-65nts, respectively [Fig. 1F]) was ~4-5-fold higher than that for N and the 65-nt poly(A) tail, suggesting that N protein has greater binding affinity for a poly(A) sequence than a non-poly(A) sequence containing various types of nucleotides. Together, the results further suggest that coronavirus N protein, similar to PABP, binds to the poly(A) tail with high affinity.

N protein is able to compete with PABP for binding to the poly(A) tail *in vitro* and in cells. To address the question of whether N protein is able to compete with PABP for binding to the poly(A) tail in an environment in which they coexist *in vitro*, the ^{32}P-labeled poly(A) tail RNA probe was incubated with mixtures containing various molar ratios of N protein to PABP, followed by EMSA. The EMSA results of N protein or PABP binding to the poly(A) tail and the relative binding percentage are illustrated in the upper and lower portions of Fig. 2A, respectively. As shown in Fig. 2A, upper portion, at molar ratios of N/PABP from 65.6 to 5.7 in lanes 3 to 7 (with the increase of PABP), minor (complex 1, indicated by the white dot in lane 3) and major (indicated by the white asterisk in lane 3) RNA-protein complexes were observed. Since the major complexes in lanes 3 to 7 corresponded to N-RNA complex in lane 2, the preferential binding of the 65-nt poly(A) tail to N protein was determined at molar ratios between 5.7 and 65.6. With further increase of PABP (i.e., decreased molar ratio of N/PABP from 4.0 to 1.9 in lanes 8 to 10), the minor complex (complex 1, indicated by the white dot in lane 3) in lanes 3 to 7 became the major complex in lanes 8 to 10, suggesting that the major complex (complex 1) consists of PABP and the 65-nt poly(A) tail. Furthermore, with the increase of PABP in lanes 11 to 13, complex 1 almost disappeared; however, complex 2 appeared, which corresponded to the PABP-RNA complex in lane 14. Since the major complex in lanes 8 to 13 consists of PABP and the 65-nt poly(A) tail, the preferential binding of the 65-nt poly(A) tail to PABP was determined at molar ratios between 0.6 and 4.0 (lanes 8 to 13). Note that a small amount of N protein (~15% [Fig. 2A, lower portion]) still bound to the poly(A) tail when the molar ratio of N protein to PABP was from 3.0 to 4.0 (lanes 8 and 9). Based on these results, it was concluded that

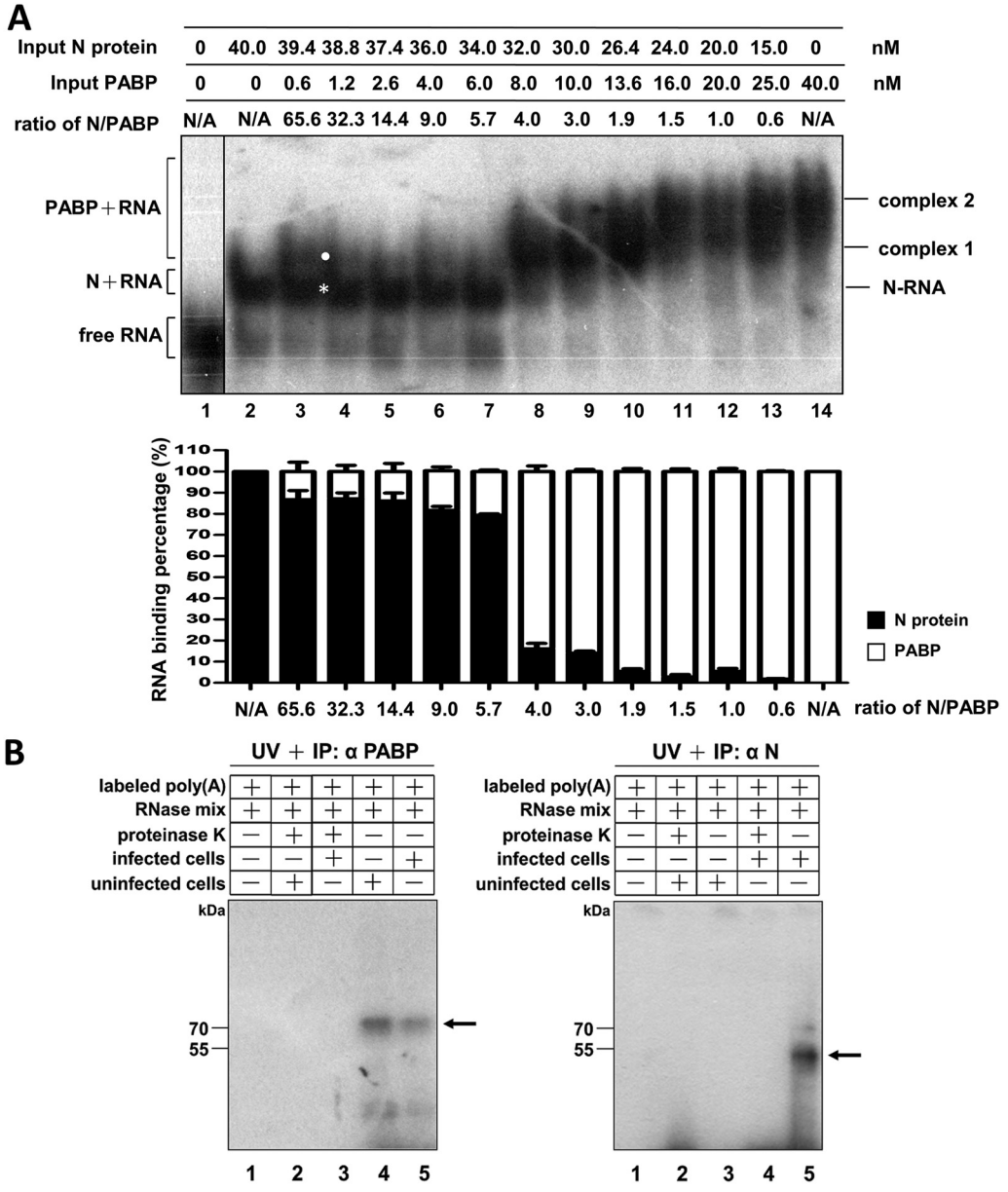

FIG 2 N protein competes with PABP for binding to the poly(A) tail. (A) (Top) *In vitro* analysis for preferential binding of the ^{32}P-labeled 65-nt poly(A) tail in an environment containing various molar ratios of N protein to PABP by EMSA (lanes 2 to 14). Lane 1, ^{32}P-labeled RNA only. Gels were spliced for labeling purposes. (Bottom) The relative binding percentages of N protein and PABP with the poly(A) tail were determined according to the results shown in the top portion. N/A, not applicable. (B) Identification of the binding of PABP and N protein with poly(A) tail *in vivo*. The ^{32}P-labeled 65-nt poly(A) tail was transfected into cells, followed by UV cross-linking and immunoprecipitation (IP) using an anti-PABP (left) or anti-N protein (right) antibody. The resulting products were analyzed by SDS-PAGE and autoradiographed. Values in panel A represent means ± SD from three independent experiments.

N protein can compete with PABP for binding to the poly(A) tail *in vitro*, even though at the same molar ratio (lane 12), PABP exhibits better binding affinity to poly(A) tails than N protein.

To determine whether N protein is able to bind to poly(A) tail in infected cells, the ^{32}P-labeled 65-nt poly(A) tail was transfected into BCoV- or mock-infected cells and UV cross-linked. Cell lysates were collected and an antibody against PABP or N protein was employed to immunoprecipitate PABP or N protein, followed by RNase treatment. As shown in Fig. 2B, left panel, antibody against PABP immunoprecipitated an ~70-kDa protein from mock-infected and BCoV-infected cells (lanes 4 and 5, respectively);

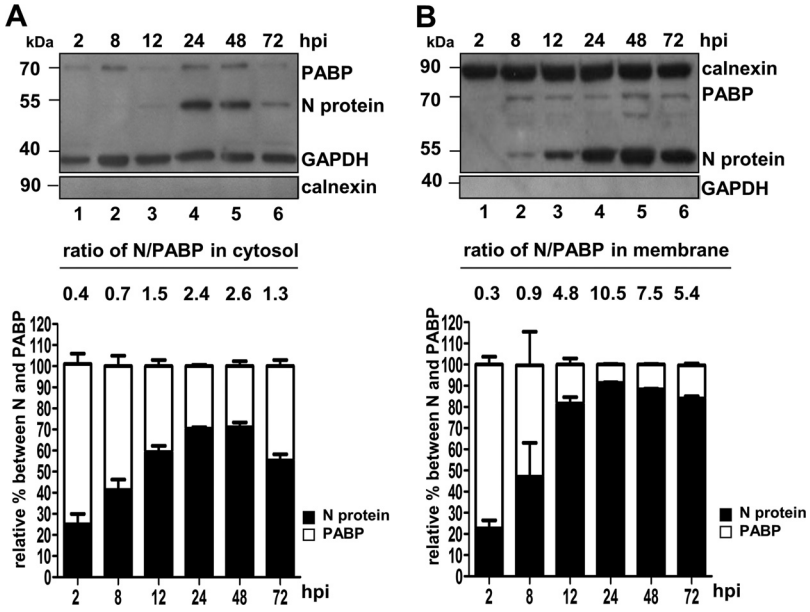

FIG 3 Molar ratio of N protein to PABP in subcellular fractions during infection. (Top) N protein and PABP immunobloting analysis for the cytosol (A) or membrane (B). (Middle and bottom) Molar ratios of N protein to PABP and relative percentages between N protein and PABP, respectively. The amounts of N protein and PABP were measured as follows. Different known concentrations of N protein and PABP were identified by immunoblotting using antibodies against both N protein and PABP. The signals were scanned densitometrically and then plotted against the concentration to obtain a standard curve for the quantitation of N protein and PABP shown at the top. Values represent means ± SD from three independent experiments. hpi, hours postinfection.

however, in Fig. 2B, right portion, antibody against N protein immunoprecipitated an ~50-kDa protein from a BCoV-infected cell (lane 5) but not the mock-infected cell (lane 3). The results suggest that in addition to PABP, N protein is able to bind to the poly(A) tail in infected cells.

Determination of molar ratio of N protein to PABP in subcellular locations at different stages of infection. As shown in Fig. 2A, the molar ratio of N protein to PABP plays a role in poly(A) tail binding preference. In addition, it has been suggested that coronavirus replication can occur in a modified membrane-associated compartment (32). It was therefore speculated that molar ratios in subcellular locations of coronavirus-infected cells at different stages of infection may also be decisive regarding PABP or N protein binding preference for the poly(A) tail. Thus, subcellular fractions of the cytosol and membrane were obtained at various time points of infection, and the amounts of N protein and PABP in each cellular fraction according to immunoblotting (Fig. 3A and B, upper portions) were quantified based on a standard curve obtained from known amounts of the proteins. As shown in Fig. 3A and B, middle and lower portions, the molar ratio of N protein to PABP in both the cytosol and membrane was low (~0.4) during the initial infection but increased (from ~0.4 to ~2.6 in the cytosol and from ~0.3 to ~10.5 in the membrane) at later infection stages. The results indicate that the amounts of N protein are increased in the both cytosol and membrane at the later time points of infection. Thus, based on the results shown in Fig. 2 and 3, we speculate that the poly(A) tail may preferentially bind with PABP during the initial infection but with N protein in the later infection, especially in membrane-associated structures.

BCoV N protein inhibits viral translation both *in vitro* and *in vivo*. Because the poly(A) tail is able to bind to N protein with high affinity (Fig. 1) and in infected cells (Fig. 2), we hypothesized that such binding may prevent the poly(A) tail on coronavirus RNA from interacting with translation factors, leading to translation inhibition. To test the hypothesis, a BCoV defective interfering (DI) RNA, a surrogate for the coronavirus

genome that has been extensively used for studies of coronavirus gene expression (33–37) (Fig. 4A), was engineered to express enhanced green fluorescent protein (EGFP); the construct was designated DI-EGFP. For *in vitro* translation analysis, DI-EGFP with the 65-nt poly(A) tail was first incubated with various amounts of N protein (Fig. 4B) for 15 min to allow the binding of N protein to the 65-nt poly(A) tail on DI-EGFP and then added to a rabbit reticulocyte lysate (RRL) for another 90 min. A similar experiment was performed in which DI-EGFP was first incubated with PABP or GST. As shown in Fig. 4B, translation of DI-EGFP with the 65-nt poly(A) tail was inhibited with increasing amounts of N protein but not PABP or GST (data not shown). To test whether the inhibition was due to the effect of N protein on the RRL, various amounts of N protein were first incubated with RRL for 60 min, and then DI-EGFP with the 65-nt poly(A) tail was added. The translation efficiency of DI-EGFP, however, was not altered (data not shown), indicating that N protein at these concentrations had no effect on the translation efficiency of RRL. Accordingly, the reduced translation efficiency shown in Fig. 4B was due to the binding of N protein with DI-EGFP but not the effect of N protein on RRL. Furthermore, it has been shown that translation using RRL still occurs with an mRNA lacking a poly(A) tail, although the translation efficiency is affected (38). Consequently, we hypothesized that if the decreased translation efficiency was due to the binding of N protein to the poly(A) tail, translation efficiency of poly(A)-deficient DI-EGFP is not altered with increasing amounts of N protein. To test this, poly(A)-deficient DI-EGFP was generated, incubated with various amounts of N protein for 15 min, and then added to the RRL. As shown in Fig. 4C, the translation efficiency was not significantly affected with increasing amounts of N protein, suggesting that the decreased translation in Fig. 4B may have been mostly due to the interaction between N protein and poly(A) tail. Because N protein apparently had no effect on the translation efficiency of RRL (data not shown) and on translation efficiency of poly(A)-deficient DI-EGFP (Fig. 4C), the inhibitory effect of translation shown in Fig. 4B may be attributed to interaction between the poly(A) tail and N protein. Note that after *in vitro* translation in RRL the amounts of DI-EGFP at various concentrations of N protein were not significantly altered, indicating that the stability of DI-EGFP is not a factor affecting the translation efficiency. It was therefore concluded that N protein is able to inhibit viral translation by binding to the viral poly(A) tail *in vitro*.

To further assess whether translation inhibition by N protein also occurs *in vivo*, the N protein or His–β-actin transcript was transfected into HEK-293T cells, followed by transfection of DI-EGFP with the 65-nt poly(A) tail (Fig. 4D, left portion) or by infection of BCoV (Fig. 4F, left portion). Cell lysates were harvested and analyzed by immunoblotting to quantitate the translation efficiency of DI-EGFP and coronavirus nsp1 (representing genome expression). As shown in Fig. 4D, right portion, and Fig. 4E, inhibition of the DI-EGFP translation was observable in cells transfected with the N protein transcript at 3, 8, and 16 h in comparison with those transfected with the His–β-actin transcript, suggesting that N protein is able to inhibit translation of DI-EGFP *in vivo*. Similar inhibition results were also obtained for cells infected with BCoV (Fig. 4F, right portion, and Fig. 4G), suggesting that N protein can inhibit translation of the coronavirus genome. Note that the levels of DI-EGFP RNA (Fig. 4D) and viral genomic RNA (Fig. 4F) were similar between the groups at the same time point, as confirmed by reverse transcription-quantitative PCR (RT-qPCR) (data not shown). Therefore, based on the results for the *in vivo* binding of N protein to poly(A) tail (Fig. 2B) and the *in vitro* analyses shown in Fig. 4B and C, the inhibitory effect of N protein on translation of DI-EGFP and BCoV *in vivo* may be at least partly attributable to the binding of N protein to the poly(A) tail on DI-EGFP and the BCoV genome.

BCoV N protein modulates translation of host mRNAs both *in vitro* and *in vivo*. To examine whether the binding of N protein to the poly(A) tail of mRNA also inhibits host mRNA translation, a β-actin transcript with the 65-nt poly(A) tail was first incubated with N protein to form an N protein-poly(A) complex and then subjected to an *in vitro* translation assay with the RRL. As shown in Fig. 5A, expression of β-actin transcripts was inhibited with increasing amounts of N protein. As with the *in vitro*

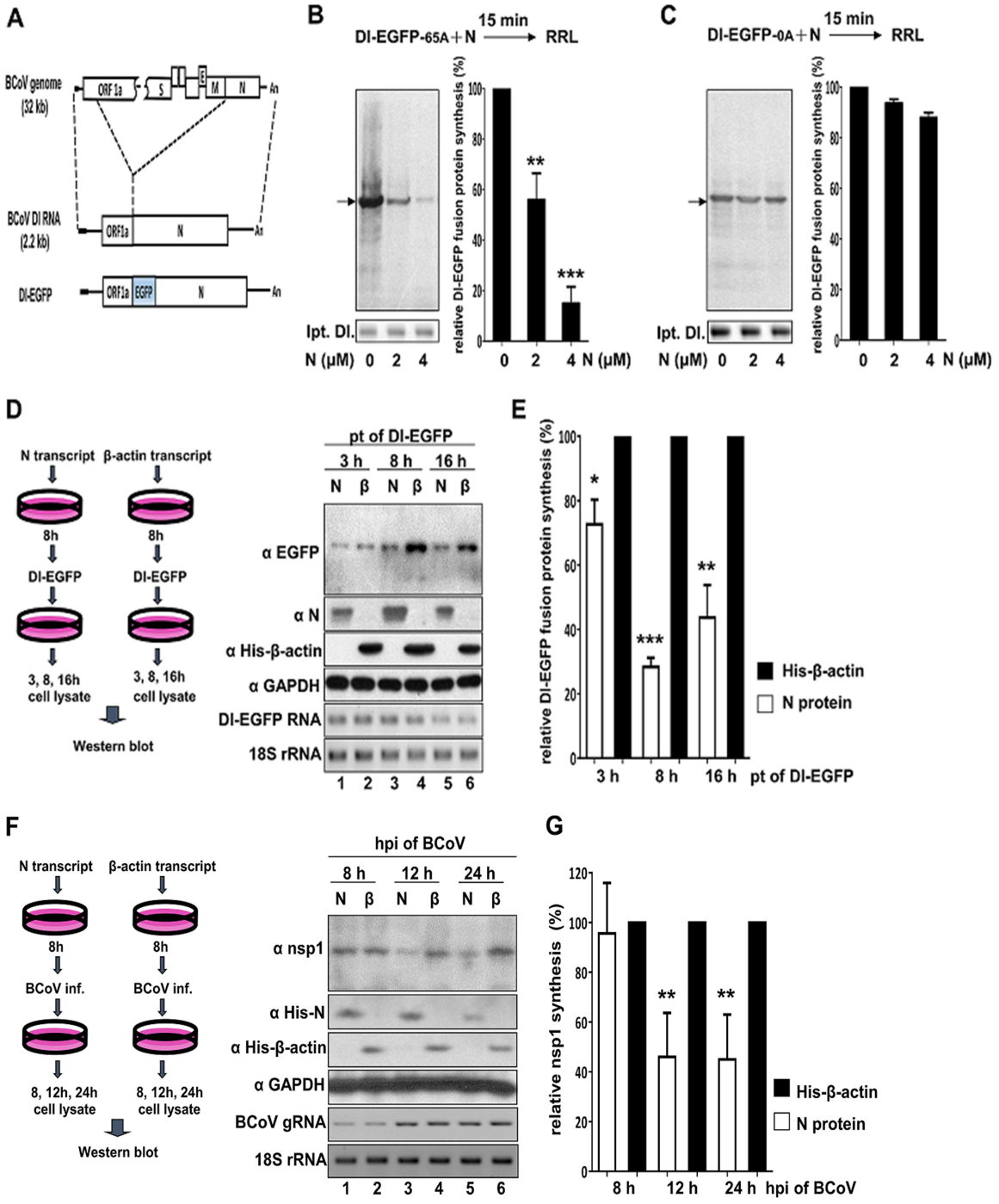

FIG 4 Translation inhibition of coronaviral RNA by N protein. (A) Diagram of the BCoV genome, BCoV DI RNA, and its derivative DI-EGFP. DI-EGFP was employed for the following translation analyses. (B) (Left) *In vitro*-synthesized fusion protein (top) from 1 μg of input DI-EGFP RNA transcript with the 65-nt poly(A) tail (Ipt. DI.) (middle), which was preincubated first with 0, 2, and 4 μM N protein (bottom) and then subjected to *in vitro* translation in RRL. (Right) Relative levels of *in vitro*-synthesized DI-EGFP fusion protein. The values shown are relative to the amount of synthesis in the absence of N protein (i.e., 0 μM N protein). (C) (Left) *In vitro*-synthesized fusion protein (top) from 1 μg of input poly(A) tail-deficient DI-EGFP RNA transcript (middle), which was preincubated with 0, 2, and 4 μM N protein (bottom) and then subjected to *in vitro* translation in RRL. (Right) Relative levels of *in vitro*-synthesized DI-EGFP fusion protein. The values shown are relative to the amount of synthesis in the absence of N protein (i.e., 0 μM N protein). (D) (Left) Diagram showing the experimental procedures to determine the effect of N protein on the translation efficiency of DI-EGFP [with 65-nt poly(A) tail] *in vivo*. (Right) Immunoblot showing the synthesis of the fusion protein from DI-EGFP in the presence of N protein or His–β-actin at different times posttransfection. The levels of DI-EGFP RNA and 18S rRNA were similar between the groups at the same time point as quantified by RT-qPCR. (E) Relative levels of *in vivo* fusion protein synthesis based on the results of the right side in panel D. The values shown are relative to the amount of synthesis in the presence of His–β-actin at each time point. (F) (Left) Diagram showing the experimental procedures to determine the effect of N protein on the translation efficiency of BCoV nsp1 *in vivo*. (Right) Immunoblot showing the synthesis of BCoV nsp1 in the presence of N

(Continued on next page)

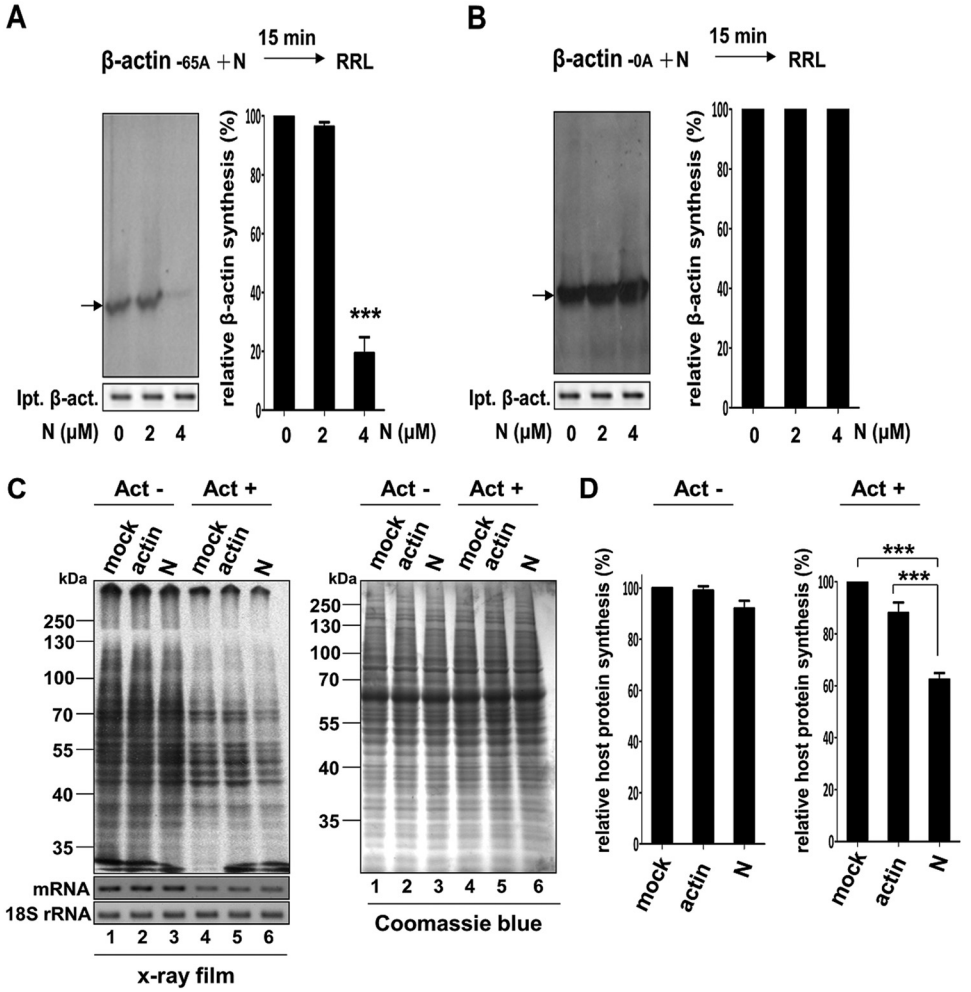

FIG 5 Translation inhibition of cellular mRNA by N protein. (A) (Left) *In vitro*-synthesized β-actin (top) from 1 μg of input β-actin RNA transcript with the 65-nt poly(A) tail (lpt. β-act.) (middle), which was preincubated with 0, 2, and 4 μM N protein (bottom) and then subjected to *in vitro* translation in RRL. (Right) Relative levels of *in vitro*-synthesized β-actin. The values shown are relative to the amount of synthesis in the absence of N protein (i.e., 0 μM N protein). (B) (Left) *In vitro*-synthesized β-actin (top) from 1 μg of the input poly(A) tail-deficient β-actin RNA transcript (middle), which was preincubated with 0, 2, and 4 μM N protein (bottom) and then subjected to *in vitro* translation in RRL. (Right) Relative levels of *in vitro*-synthesized β-actin. The values shown are relative to the amount of synthesis in the absence of N protein (i.e., 0 μM N protein). (C) Effect of expressed N protein on translation of host mRNAs *in vivo*. After mock transfection or independent transfection of His–β-actin and N protein RNA transcripts into HEK-293T cells in the absence or presence of actinomycin D followed by [^{35}S]methionine, equal amounts of cell lysate were analyzed by SDS-PAGE and exposed to X-ray film (left) or stained with Coomassie blue (right). The levels of host mRNA (represented by GAPDH mRNA) and 18S rRNA shown on the left were quantified by RT-qPCR. (D) Relative levels of host protein synthesis based on the results on the left side of panel C. The values shown are relative to the amount of synthesis in the absence of transfection (i.e., mock transfection). Values in panels A, B, and D represent the means $\pm$ SD from three independent experiments. ***, $P < 0.001$ (unpaired Student's *t* test).

translation assay for DI-EGFP (Fig. 4), to further determine whether the inhibitory effect was due to the binding of N protein to the poly(A) tail, a poly(A) tail-deficient β-actin transcript was first incubated with various amounts of N protein, followed by the assay. However, inhibition was not observed (Fig. 5B), as no significant difference in expres-

FIG 4 Legend (Continued)
protein or His-β-actin at different times posttransfection. The levels of viral genome (BCoV gRNA) and 18S rRNA were similar between the groups at the same time point as quantified by RT-qPCR. (G) Relative levels of BCoV nsp1 *in vivo* based on the results on the right side in panel F. The values shown are relative to the amount of synthesis in the presence of His–β-actin at each time point. Values in panels B, C, E, and G represent means $\pm$ SD from three independent experiments. *, $P < 0.05$; **, $P < 0.01$; ***, $P < 0.001$ (unpaired Student's *t* test). RRL, rabbit reticulocyte lysate; pt, posttransfection; N, N protein; β, His–β-actin.

sion of the poly(A) tail-deficient β-actin transcript was observed with increasing amounts of N protein. These results (Fig. 5A and B) suggest that binding of N protein to the poly(A) tail of the β-actin transcript is a major factor leading to translation inhibition.

In addition to individual cellular mRNAs *in vitro*, inhibition of host mRNA translation by N protein was also examined globally in cells. For this, the N protein transcript or His-tagged β-actin transcript was independently transfected into HEK-293T cells for 1 h, after which the cells were incubated for 3 h in the presence or absence of actinomycin D. After addition of actinomycin D, the cells were labeled with [^{35}S]methionine for 8 h, and equal amounts of cell lysate were analyzed by SDS-PAGE. As shown in the left portions of Fig. 5C and D, inhibition of host protein synthesis was not apparent in cells not treated with actinomycin D; however, with actinomycin D treatment, synthesis of host proteins in cells transfected with the N protein transcript was decreased by approximately one-third in comparison with that in cells transfected with the His-tagged β-actin transcript or mock transfected (Fig. 5C, left portion, and Fig. 5D, right portion). The fact that the efficiency of N protein inhibition was better in actinomycin D-treated cells than in untreated cells may indicate that in the absence of nascent mRNA synthesis, expressed N protein was involved in interaction with preexisting mRNAs, leading to inhibition of host protein synthesis. In addition, the levels of host mRNA (represented by glyceraldehyde-3-phosphate dehydrogenase [GAPDH] mRNA) were similar (Fig. 5C) between the groups treated with actinomycin D, as confirmed by RT-qPCR (data not shown), and thus were not affected by the expressed N protein. Thus, it was concluded that in addition to coronaviral RNA, N protein is also able to globally inhibit host mRNA translation, and based on *in vitro* results (Fig. 5A and B), such inhibition in cells may at least partly result from the binding of N protein to the poly(A) tail.

Interactions among the poly(A) tail, N protein, and PABP. To elucidate the possible mechanism by which interactions among the poly(A) tail, N protein, and PABP regulate gene expression, we first determined whether the poly(A) tail is able to interact with both the N protein and PABP using lysates of infected cell. For this, an 84-nt biotinylated RNA, consisting of 19 non-poly(A) nucleotides (containing biotin-conjugated uridine) followed by a 65-nt poly(A) tail, was synthesized and incubated with cell lysates, followed by a streptavidin pulldown assay and immunoblotting. As shown in Fig. 6A (lane 1), both the N protein and PABP were detected (indicated by asterisks), demonstrating poly(A) tail interaction. To ensure that the detection of the N protein and PABP was in fact due to interaction with the poly(A) tail and not with the 19 non-poly(A) residues, a biotinylated RNA containing the 19 non-poly(A) nucleotides was also used. However, neither was observed (data not shown) by immunoblotting, confirming that the 65-nt poly(A) tail, and not 19 non-poly(A) nucleotides, can interact with both the N protein and PABP from infected cell lysates. We next addressed whether the N protein is able to directly bind to the PABP by performing a pulldown assay in which purified His-tagged PABP (Fig. 6B, left portion) was bound to nickel-nitrilotriacetic acid (Ni-NTA) beads and mixed with purified untagged N protein (Fig. 6B, right portion). As shown in Fig. 6C, untagged N protein (left portion, lane 1) was copelleted by His-tagged PABP, suggesting that the N protein can physically bind to the PABP. Finally, we assessed whether the N protein is able to interact with the PABP from infected cell lysates by incubating Ni-NTA beads with His-tagged N protein and infected cell lysates and subjecting the eluate to immunoblotting with an antibody against PABP. As shown in Fig. 6D, a signal at ~70 kDa representing the cellular PABP was observed (left portion, lane 1), suggesting that the N protein is able to interact with cellular PABP from infected cell lysates. Consistently, the reciprocal pulldown assay with His-tagged PABP demonstrated that the PABP can interact with the N protein from infected cell lysates (Fig. 6D, right portion, lane 1). To determine whether RNA bridging is essential for such interaction, RNase treatment was included in the pulldown assay. As shown in Fig. 6D, both the PABP (left portion, lane 6) and N protein (right portion,

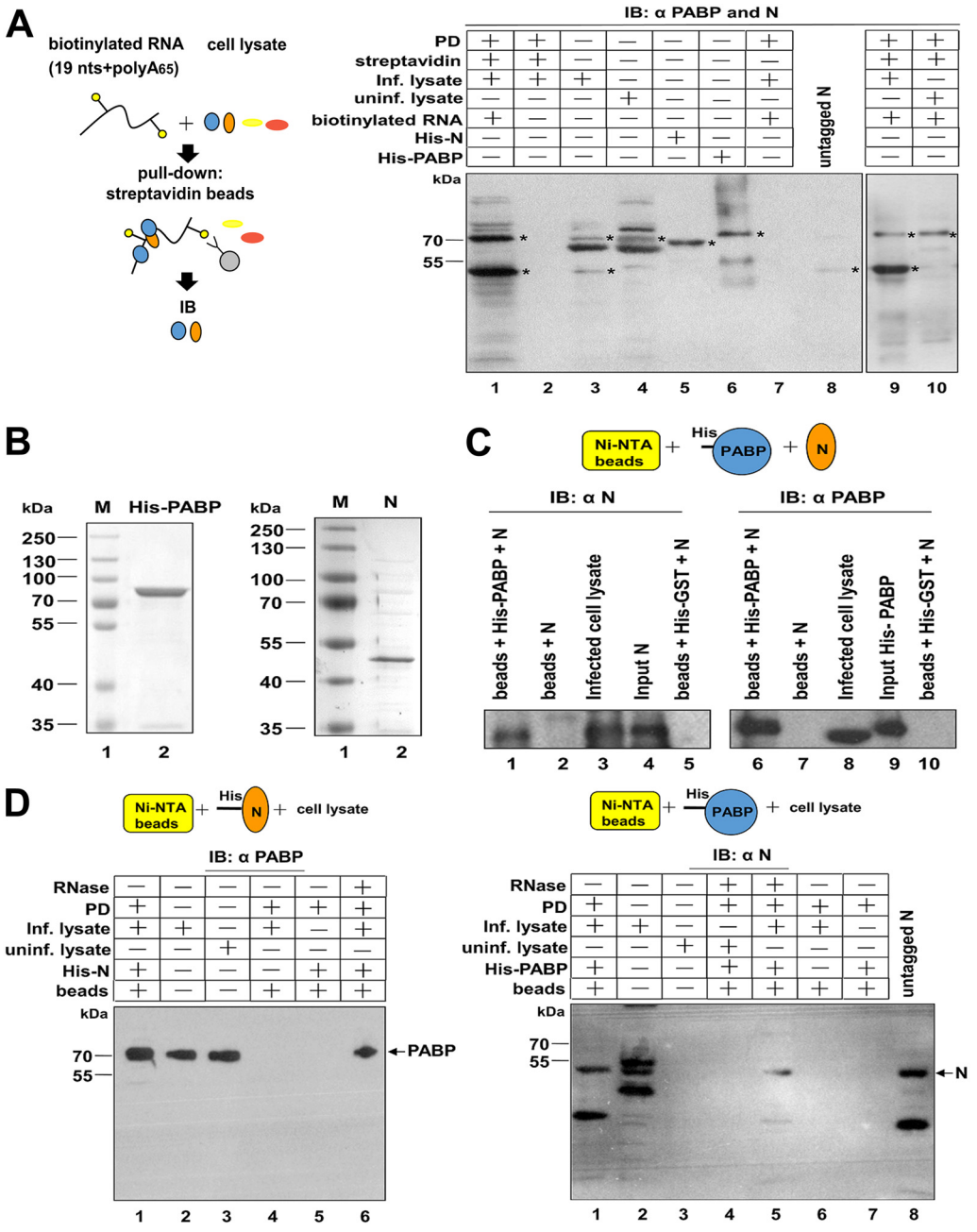

FIG 6 Interactions between the poly(A) tail, N protein, and PABP. (A) Interactions of the poly(A) tail with N protein and/or PABP in mock-infected or infected cell lysates. Proteins from mock-infected or infected cell lysates interacting with a biotinylated poly(A) tail were pulled down by streptavidin, followed by immunoblotting using antibodies against PABP and N protein. The upper and lower asterisks in lanes 1, 9 (from streptavidin pulldown samples of infected cell lysates), and 3 (from infected cell lysates) indicate cellular PABP and coronaviral N protein, respectively; the asterisk in lane 4 (from mock-infected cell lysates) indicates cellular PABP; the asterisks in lanes 5 and 6 indicate *E. coli*-expressed N protein and PABP, respectively; the asterisk in lane 7 indicates untagged N protein; and the asterisk in lane 10 (from streptavidin pulldown samples of mock-infected cell lysates) indicates cellular PABP. (B) His-tagged PABP (left) and untagged N protein (right) were expressed in *E. coli*, analyzed by SDS-PAGE, and stained with Coomassie blue. (C) Pulldown assay to determine direct binding between PABP and N protein. His-tagged PABP was bound to Ni-NTA beads and mixed with untagged N protein. The pulldown materials were detected by immunoblotting using an antibody against N protein (left) or PABP (right). (D) Pulldown assay using His-tagged N protein (left) or His-tagged PABP (right) to assess its interaction with PABP or N protein, respectively, in infected cell lysates. Bound proteins from lysates were analyzed by immunoblotting with an antibody against PABP (left) or N protein (right). The arrow indicates the position of PABP (left) and N protein (right). PD, pulldown.

lane 5) were detected, suggesting that RNA bridging is not a requirement for the interaction between the two proteins. It was concluded that the poly(A) tail can interact with both the N protein and PABP from infected cell lysates. In addition, the N protein is able to physically bind to the PABP *in vitro* and to interact with PABP from infected cell lysates.

Interactions of the poly(A) tail and N protein with translation factor eIF4G and coronavirus replicase protein nsp9. To further examine the role of the poly(A) tail and N protein in gene regulation, we first determined whether the poly(A) tail is able to interact with eIF4G and nsp9, a coronavirus replicase protein that is associated with polymerase nsp12 (20), is essential for replication (21), and is involved in the initiation of negative-strand RNA synthesis (22). To this end, the 84-nt biotinylated RNA described above [consisting of 19 non-poly(A) nucleotides followed by the 65-nt poly(A) tail] was used in the streptavidin pulldown assay. As shown in Fig. 7A, both eIF4G (left portion, lane 1) and coronavirus nsp9 (right portion, lane 1) were detected by immunoblotting, though they were not observed with the biotinylated RNA containing only the 19 non-poly(A) tail nucleotides (data not shown), suggesting that the 65-nt poly(A) tail is able to interact with eIF4G and coronavirus nsp9 from infected cell lysates. We next performed the pulldown assay with Ni-NTA beads to determine whether the N protein is able to interact with eIF4G in infected cells. In this case, eIF4G was not detected when using infected cell lysates treated with RNase or left untreated (Fig. 7B, lane 1 or 7, respectively) but was detected when using mock-infected cell lysates treated with RNase or left untreated (Fig. 7B, lane 2 or 8, respectively). To address whether the lack of eIF4G detection was due to the His-tagged N protein being outcompeted by endogenous N in infected cell lysates, a pulldown assay with protein G beads followed by incubation with an antibody against N protein was employed. Indeed, eIF4G was detected in the absence or presence of RNase (Fig. 7C, lane 1 or 6, respectively), suggesting that the N protein can interact with eIF4G from infected cell lysates without the assistance of RNA. Our results show that the N protein is able to bind to the poly(A) tail, yet it is possible that at least a portion of the detected coronavirus nsp9 in Fig. 7A is due to its interaction with the N protein. Another pulldown assay was performed to investigate this possibility. As shown in Fig. 7D, lane 2 and lane 7, nsp9 was detected in infected cell lysates in the absence or presence of RNase treatment, respectively, suggesting that the N protein is able to interact with nsp9 without an RNA bridge. These data suggest that both the poly(A) tail and N protein are able to interact with the translation factor eIF4G and replicase protein nsp9.

Poly(A)-bound N protein interacts efficiently with eIF4G but not eIF4E. To further examine the translation inhibition caused by binding of the N protein to the poly(A) tail, we next assessed whether N can interact with the translation factor eIF4E. For this, a fixed concentration of biotinylated RNA consisting of 19 non-poly(A) nucleotides followed by the 65-nt poly(A) tail was first incubated with increasing amounts of N protein (2, 4, and 6 μM) and then with mock-infected cell lysates followed by a streptavidin pulldown assay. In this context, the N protein interacted with eIF4G efficiently (Fig. 8A, lanes 4 to 6, blot 1), whereas the amount of eIF4E detected decreased (Fig. 8A, lanes 4 to 6, blot 2) with an increase in N protein (Fig. 8A, lanes 4 to 6, blot 4), suggesting that the poly(A)-bound N protein cannot interact efficiently with eIF4E. Note that the binding efficiency between the aforementioned biotinylated RNA and the input PABP or N protein increased with increasing amounts of input PABP and N protein, as confirmed by immunoblotting shown in blots 3 (lanes 1 to 3) and 4 (lanes 4 to 6), respectively. With regard to the observed eIF4E (Fig. 8A, lane 4, blot 2), we interpret that the biotinylated poly(A) tail not bound to N protein, which resulted from insufficient binding of N protein to the biotinylated poly(A) tail due to the reduced amount of input N protein (2 μM), was still able to bind to PABP and then eIF4G and eIF4E, leading to detection of eIF4E (Fig. 8A, lane 4, blot 2). Accordingly, with an increasing amount of input N protein, the biotinylated poly(A) tail was almost all bound

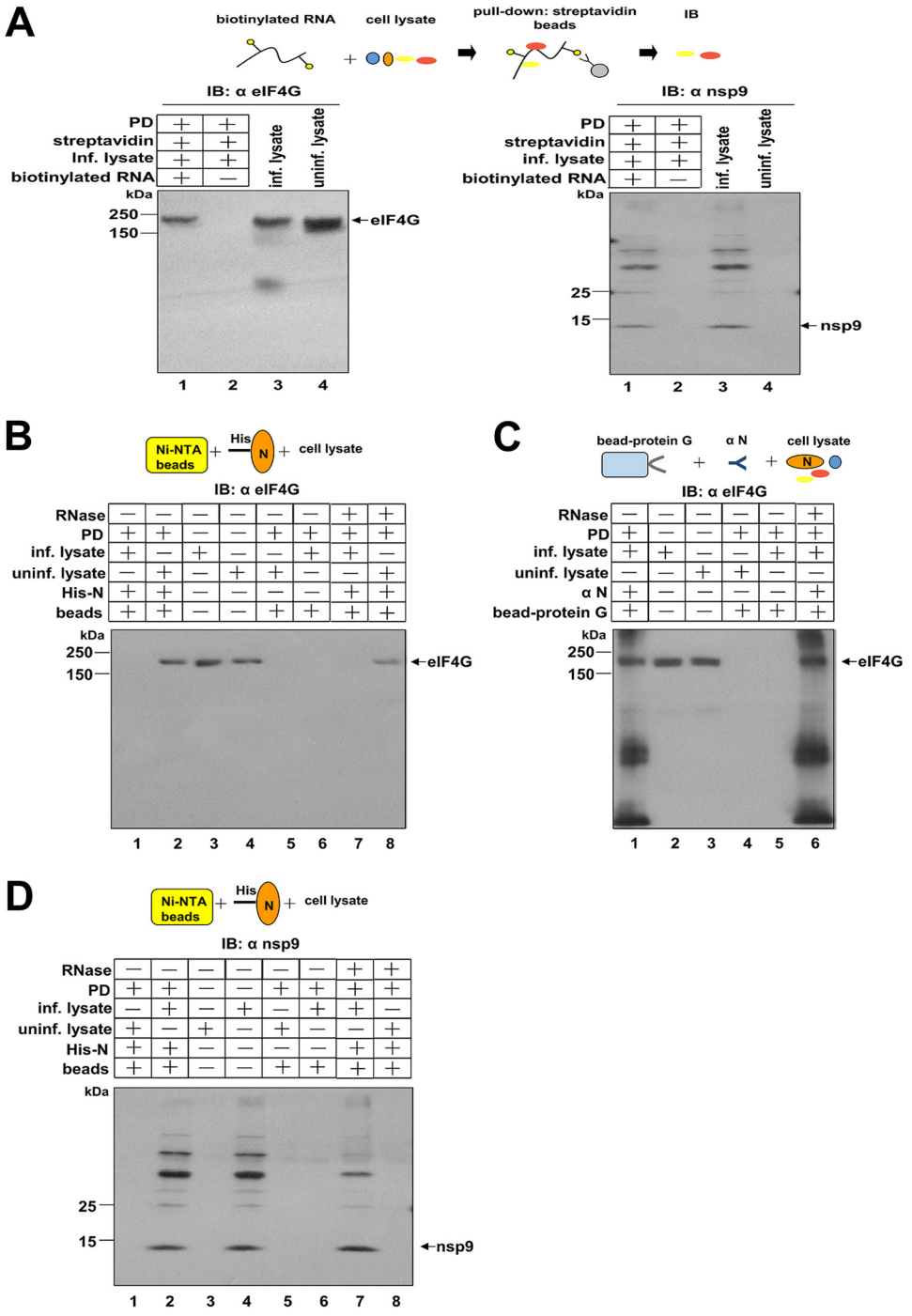

FIG 7 Interactions of poly(A) tail and N protein with cellular eIF4G and coronavirus nsp9. (A) The poly(A) tail interacts with cellular eIF4G and coronavirus nsp9. Infected cell lysates were incubated with the biotinylated poly(A) tail and pulled down by streptavidin, followed by immunoblotting with antibodies against eIF4G (left) and nsp9 (right). Coronavirus nsp9 (12 kDa) and cellular eIF4G (220 kDa), indicated by an arrow in lane 1 in the left and right blots, respectively, were identified. (B) Ni-NTA bead pulldown assay using the His-tagged N protein followed by immunoblotting with an antibody against eIF4G to determine interaction between N protein and eIF4G. The arrow indicates the position of 220-kDa eIF4G. (C) Protein G bead pulldown assay followed by immunoblotting with an antibody against eIF4G to determine interaction between N protein and eIF4G. The arrow indicates the position of 220-kDa eIF4G. (D) Ni-NTA bead pulldown assay using the His-tagged N protein followed by immunoblotting with an antibody against nsp9 to determine interaction between N protein and nsp9. The arrow indicates the position of 12-kDa nsp9.

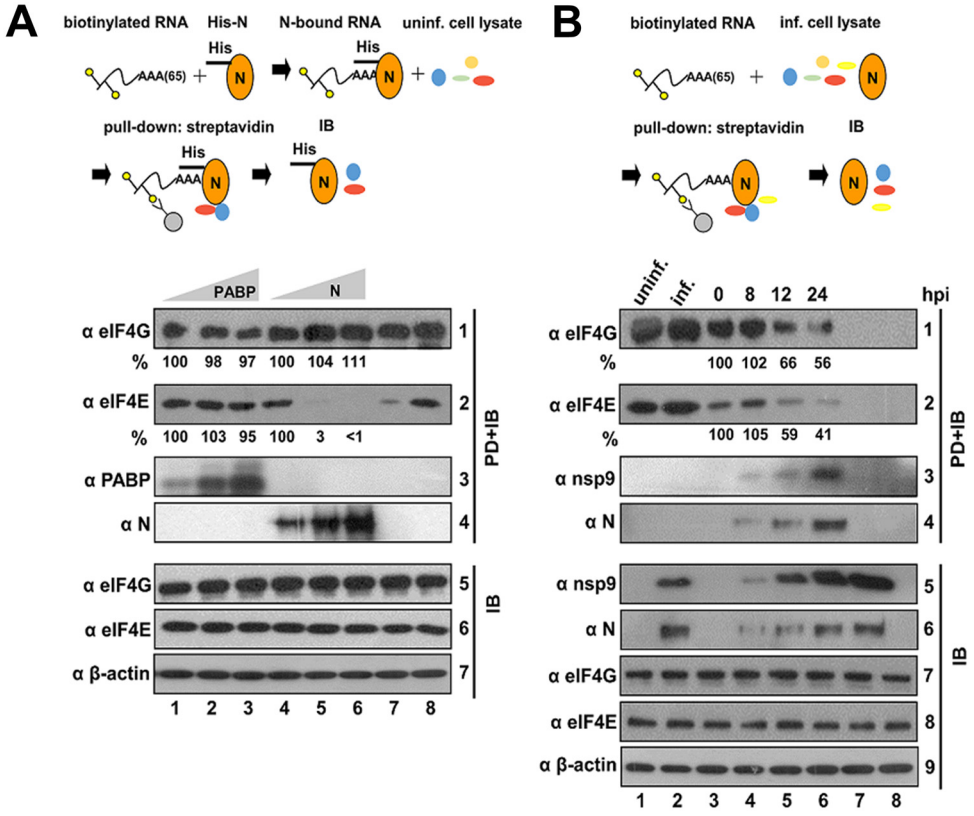

FIG 8 Interactions of the poly(A) tail and N protein with cellular eIF4E. (A) Interaction of the poly(A) tail-bound N protein with eIF4G and eIF4E in mock-infected cells. For lanes 1 to 6 in blots 1 and 2, a fixed concentration (25 nM) of biotinylated RNA consisting of 19 non-poly(A) nucleotides followed by the 65-nt poly(A) tail was first incubated with increasing amounts (2, 4, and 6 μM) of PABP (lanes 1 to 3) or N protein (lanes 4 to 6) and then with mock-infected cell lysates, followed by a streptavidin pulldown assay and immunoblotting. Values in blots 1 and 2 represent the mean percentages from three independent experiments, but SD are not shown. Lanes 1 to 6 in blots 3 and 4 show detection of input PABP (blot 3) and N protein (blot 4) bound by biotinylated RNA. A fixed concentration (25 nM) of biotinylated RNA consisting of 19 non-poly(A) nucleotides followed by the 65-nt poly(A) tail was incubated with increased amounts (2, 4, and 6 μM) of PABP (lanes 1 to 3) or N protein (lanes 4 to 6), followed by a streptavidin pulldown assay and immunoblotting. Lanes 1 to 6 in blots 5 and 6 show detection of eIF4G and eIF4E by immunoblotting from uninfected cell lysates used for the aforementioned streptavidin pulldown assay. For lane 7 in blots 1 and 2, the N protein was incubated with mock-infected cell lysates, followed by an Ni-NTA bead pulldown assay and immunoblotting. For lane 8 in blots 1 and 2, biotinylated RNA consisting of 19 non-poly(A) nucleotides followed by the 65-nt poly(A) tail was incubated with mock-infected cell lysates, followed by a streptavidin pulldown assay and immunoblotting. Lanes 7 and 8 in blots 5 and 6 show detection of eIF4G and eIF4E from mock-infected cell lysates used for the aforementioned Ni-NTA bead (lane 7) or streptavidin (lane 8) pulldown assay by immunoblotting. (B) Interaction of the poly(A) tail with eIF4G and eIF4E in BCoV-infected cells. For lanes 3 to 6 in blots 1 to 4, biotinylated RNA consisting of 19 non-poly(A) nucleotides followed by the 65-nt poly(A) tail was incubated with BCoV-infected cell lysates collected at 0, 8, 16, and 24 hpi, followed by a streptavidin pulldown assay and immunoblotting. Lane 1 contained uninfected cell lysates only; lane 2 contained infected cell lysates only. For lanes 7 and 8, the streptavidin beads were incubated with infected (lane 7) or uninfected (lane 8) cell lysates, followed by a streptavidin pulldown assay and immunoblotting. Values in blots 1 and 2 represent mean percentages from three independent experiments, but SD are not shown. Blots 5 and 8 show detection of N protein, nsp9, eIF4G, and eIF4E by immunoblotting from uninfected or infected cell lysates used for the aforementioned streptavidin pulldown assay.

and thus was unable to interact with eIF4E (Fig. 8A, lanes 5 to 6, blot 2), supporting the above argument.

To further determine whether the poly(A) tail is able to interact with eIF4G, eIF4E, and replication factor nsp9 in infected cells, lysates at different time points of coronavirus infection were incubated with a biotinylated RNA consisting of 19 non-poly(A) nucleotides and then the 65-nt poly(A) tail, followed by streptavidin pulldown. As shown in Fig. 8B, levels of eIF4G and eIF4E were decreased (lanes 4 to 6, blots 1 and 2, respectively) with increasing N protein (lanes 4 to 6, blot 4), whereas nsp9 was increased (lanes 4 to 6, blot 3). These results suggest that in infected cells, the poly(A)

tail is able to interact with eIF4G and eIF4E but that the efficiency is decreased with increasing amounts of N protein. Because the N protein can interact with coronaviral replicase proteins (8–14), we speculate that these viral proteins compete with eIF4G for interaction with N in infected cells, which in our assay would lead to reduced detection of eIF4G. This argument is supported by the increased amounts of nsp9 detected (Fig. 8B, lanes 4 to 6, blot 3), which is also able to interact with the N protein (Fig. 7). Furthermore, the amount of eIF4E detected (Fig. 8B, lanes 4 to 6, blot 2) may be attributed to the input biotinylated poly(A) tail being bound by PABP followed by eIF4G and eIF4E. In line with this argument, the reduced amount of eIF4E detected (Fig. 8B, lanes 4 to 6, blot 2) may have resulted from the increased level of poly(A)-bound N protein, which, based on the results shown in Fig. 8A, cannot interact with eIF4E. Together, the poor interaction efficiency between the poly(A)-bound N protein and eIF4E (Fig. 8A) and the decreased interaction efficiency between the poly(A) tail and eIF4G and eIF4E in infected cells (Fig. 8B) may explain the results of decreased translation efficiency observed in coronaviruses and host cells (Fig. 4 and 5).

DISCUSSION

Here we provide evidence for interactions among the poly(A) tail, N protein, and PABP both *in vitro* and in infected cells. We also demonstrate that poly(A) tail binding by the N protein inhibits translation of both coronaviral RNA and host mRNA. Further examination revealed that both the poly(A) tail and N protein are able to interact with the translation factor eIF4G and replicase protein nsp9. However, the poly(A)-bound N protein cannot interact efficiently with eIF4E. The mechanism by which the aforementioned interactions regulate gene expression in coronaviruses and host cells and the biological relevance of such interactions are discussed below.

It has been demonstrated that the binding of PABP to a poly(A) tail (39) followed by eIF4G and eIF4E binding to form a translation initiation complex is required for efficient protein synthesis. In the current study, we showed that an N protein-bound poly(A) tail can interact with eIF4G but largely cannot interact with eIF4E (Fig. 8). Therefore, such an inefficient interaction may affect the constitution of a stable translation initiation complex, leading to decreased translation efficiency, as shown in Fig. 4 and 5. It is known that eIF4G can bind to eIF4E; however, the mechanism by which the poly(A)-bound N protein is able to interact with eIF4G but not with eIF4E remains to be experimentally elucidated. It has been suggested that allosteric interactions mediated by the poly(A) tail, PABP, eIF4G, and eIF4E are critical for translation initiation (39–41) and that molecules such as 4EGI-1 (42) and eIF4E-binding proteins (4EBPs) (43) are also involved in these interactions. Therefore, it is possible that binding of the N protein to eIF4G may cause a conformational change in eIF4G and thus decrease the binding efficiency with eIF4E. Alternatively, the N protein may use the same binding site as utilized for eIF4E to bind to eIF4G; thus, once eIF4G is bound to the N protein, eIF4G cannot bind to eIF4E, leading to undetectable eIF4E in pulldown assays. These arguments are in agreement with results of an *in vitro* translation assay (Fig. 4B and 5A) in which the poly(A) tail was first bound by the N protein, resulting in decreased translation efficiency. Accordingly, such a mechanism [binding of N to the poly(A) tail] may explain, in part, why translation was inhibited in cells (Fig. 4D to G and 5C and D). To our knowledge, the translation inhibition caused by the binding of N to the poly(A) tail has not been previously documented for coronaviruses.

Regarding cellular mRNA, as argued above, binding of N to the poly(A) tail can inhibit translation, possibly preventing the use of mRNA for gene expression. Nevertheless, the outcome of such binding may not be applicable to coronavirus genomic RNA and subgenomic mRNA (sgmRNA) because the N protein can interact with viral replicase proteins (8–14) and nsp9 (Fig. 7). We speculate that in addition to translation inhibition, N protein binding to the poly(A) tail followed by interaction with replicase protein may be a highly important task for coronavirus RNA species, including sgmRNA (44). Thus, further study is required to demonstrate the biological relevance of the interaction. One may argue that the poly(A) tail of cellular mRNA may also be bound by

the N protein, followed by interaction with these replicase proteins. However, because *cis*-acting elements located at the 5′ and 3′ termini of the coronavirus have been demonstrated to be required for coronavirus replication (45), a lack of these elements in cellular mRNA would explain the above argument.

According to the elegant model proposed by Hurst et al. (10), after release of an N protein-bound viral genome into the cell, displacement of the N protein from the 5′ two-thirds of the genome may allow replicase proteins to be translated, including nsp3. This translated nsp3 then associates with infecting (residual) N protein, which is bound to the 3′ end of the incoming viral genome, and tethers the complex to the endoplasmic reticulum (ER). Based on the results of the current study, we propose a modification of this model with more details, as follows. Because coronavirus assembly occurs at the membrane (13), where the N protein concentration is higher than that of PABP (Fig. 3), we speculate that the incoming viral genomic poly(A) tail may be bound by N protein. Additionally, because N has higher binding affinity for the poly(A) tail than for a non-poly(A) sequence (Fig. 1), it is possible that for the incoming viral genomic RNA, the N protein disassociates from all genome regions except the poly(A) tail, allowing translation of replicase proteins to occur. At this point, it can be expected that the translation efficiency may be decreased because the poly(A) tail is bound by N (Fig. 4). However, once nsp3 is synthesized, it can associate with the N protein and tether the N-poly(A)-bound genome to the replication complex at the ER (9, 10) for the first round of replication to synthesize a nascent genomic RNA and sgmRNA.

During infection, the genome of the positive-sense RNA virus functions as a template for both translation and replication; therefore, these two processes must be regulated to enable efficient gene expression. In coronaviruses, however, the mechanisms by which the two processes are regulated remain unclear. Based on the results from the current study and others, (i) the poly(A) tail can be bound by PABP and function in translation (46), (ii) the poly(A) tail is a start site for negative-strand RNA synthesis (47), (iii) the poly(A) tail can also be bound by the N protein with high affinity (Fig. 1), (iv) the N protein can interact with viral replicase proteins (8–14) and nsp9 (Fig. 5) and participates in replication (15–18), and (v) nsp9 is required for coronavirus replication (21) and is associated with the replication complex for negative-strand initiation according to the model proposed by Züst et al. (22). Altogether, we speculate that similar to the 5′-terminal cloverleaf in polioviruses (27, 28), the coronavirus 3′ poly(A) tail, which is required for both translation and replication (36, 46), may function as a regulator to coordinate utilization of the genome for translation (binding to PABP) or replication (binding to N). Further experiments are required to demonstrate whether binding of the poly(A) tail to N protein is a key step needed to regulate the two processes.

Based on the data presented herein and reported by others, a mechanism by which interactions among the poly(A) tail, PABP, and N protein regulate gene expression in coronaviruses is proposed; it is illustrated in Fig. 9. At the early stage of infection, PABP is abundant (Fig. 3). The poly(A) tail of the coronavirus genomic RNA may predominantly be bound by PABP, followed by interaction with other translation factors, such as eIF4G and eIF4E (Fig. 8), leading to translation. With an increase in N protein in the later stage of infection (Fig. 3), binding of the N protein to poly(A) tails on coronavirus genomic RNA decreases the interaction efficiency between the poly(A) tail and translation factors such as eIF4E (Fig. 8), leading to translation inhibition.

Although we understand that additional data are required to determine the role of binding of the poly(A) tail to N protein in the switch from genome translation to replication, we attempt to explain the potential gene regulation in coronaviruses based on the current findings from different viewpoints. First, in terms of an individual viral genomic RNA, binding of the poly(A) tail by PABP or the N protein may decide the subsequent function of the RNA. Second, in terms of the infection stage, the major proportion of viral RNA in the early stage of infection functions in translation via binding of the poly(A) tail by PABP, whereas in later stages, binding of the poly(A) tail by the N protein and subsequent replicase proteins downregulates translation and may

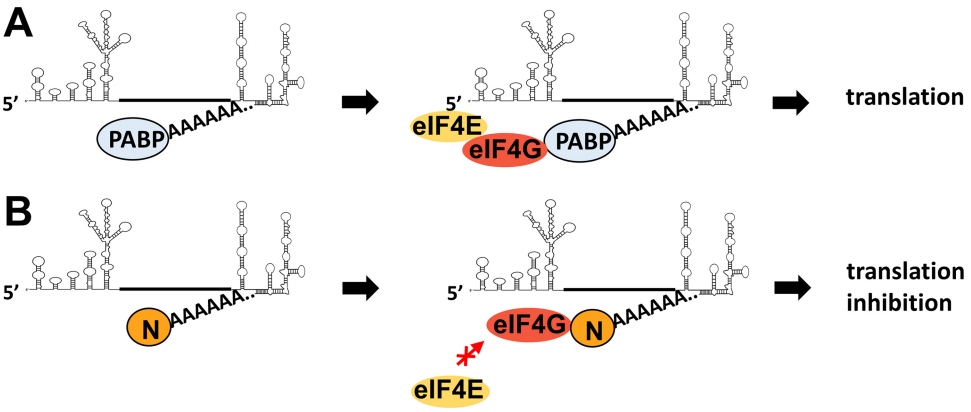

FIG 9 Proposed model for the regulation of gene expression in coronaviruses. (A) The poly(A) tail of the coronavirus genomic RNA binds to PABP followed by eIF4G and eIF4E, leading to translation. (B) N protein can bind to the poly(A) tail of coronavirus genomic RNA and interact with eIF4G but not with eIF4E, leading to translation inhibition.

lead to replication. Third, in terms of subcellular location, the N protein has been shown to accumulate at a modified membrane-associated compartment where coronavirus replication and assembly occur (32, 48). Thus, the findings of the study reporting that membrane levels of PABP are much reduced compared to those in the cytosolic fraction (49) support our results showing that a high molar ratio of N to PABP was present in the membrane fraction (Fig. 3), leading to binding of the poly(A) by the N protein and possibly thereby directing the viral RNA toward replication. In addition, we argue that the aforementioned interactions and their effects on the regulation of gene expression are stochastic, rather than an all-or-none process in the infected cells.

In conclusion, we demonstrate interactions among the poly(A) tail, N protein, and PABP, as well as those among the N protein and eIF4G and nsp9. Of the interactions shown in this study, binding of the poly(A) tail to PABP followed by eIF4G and eIF4E leads to translation. However, binding of poly(A) tail to N protein decreases the interaction efficiency between the poly(A) tail and eIF4E, leading to translation inhibition. In addition, whether binding of the poly(A) tail by the N protein followed by interaction with nsp9 may further direct viral RNA toward negative-strand RNA synthesis remains to be determined.

MATERIALS AND METHODS

Viruses, cells, and antibodies. Human rectum tumor 18 (HRT-18) and HEK-293T cells were obtained from David A. Brian (University of Tennessee) and maintained in Dulbecco's modified Eagle's medium (DMEM) supplemented with 10% fetal bovine serum (FBS; HyClone) and antibiotics at 37°C with 5% CO_2. The plaque-purified Mebus strain of BCoV (GenBank accession no. U00735) was grown on an HRT-18 cell line as described previously (50, 51). Anti-N protein (BCoV) antibody and anti-nsp9 (BCoV) antibody were obtained from David A. Brian (University of Tennessee). Antibodies used for this study are as follows: anti-EGFP antibody (GeneTex), anti-PABP antibody (Cell Signaling Technology), anti-eIF4G antibody (Cell Signaling Technology), anti-eIF4E antibody (Cell Signaling Technology), anti-GAPDH antibody (GeneTex), anti-calnexin antibody (Cell Signaling Technology), and anti-His tag antibody (Bio-Rad).

Construction of plasmids and DNA templates for RNA probes. The DNA templates 55 nt + 65A, 55 nt, 65A, 55 nt + 45A, 55 nt + 25A, 25A, and BCoV-65nts for synthesis of RNA probes were produced by PCR. The template for 65A and 25A (65 and 25 adenosine residues) were generated by PCR using a primer containing 65 and 25 thymidine nucleotides, respectively, and a primer containing T7 promoter sequence plus 3 guanosine residues. Therefore, except for 3 guanosine residues, there are no extra non-adenosine residues in both RNA probes after *in vitro* transcription. To synthesize a DNA template containing the 65-nt poly(A) tail and 19-nt non-poly(A) tail, a primer with a sequence of 5′-TGTAATACGACTCACTATAGGGCCAATTGAAGAAT-3′ and a primer with a sequence of 5′-T(65)GTGATTCTTCAATTGG-3′ were used for PCR. Constructs actin-65nts for the RNA probe and His-tagged β-actin for *in vitro* translation were amplified by RT-PCR using RNA extracted from HRT-18 cells. To construct DI-EGFP, the EGFP gene was inserted into BCoV DI RNA at the site between ORF 1a and the N protein gene. For this, a DNA fragment containing the EGFP sequence and HpaI and XbaI restriction enzyme sites was amplified by an overlap PCR mutagenesis procedure, digested with HpaI and XbaI, and ligated into HpaI- and XbaI-linearized pDrepI to create pDI-EGFP. pDI-EGFP contained full-length EGFP and N protein genes.

Expression of recombinant proteins. For His-tagged N protein, pET32aN, which contains the BCoV N protein gene, was transformed into *Escherichia coli* BL21(DE3) cells, followed by inoculation into LB medium. The cells were then induced with isopropyl thio-β-D-galactoside, harvested by centrifugation, resuspended in phosphate-buffered saline (PBS), and then sonicated. The supernatant containing the recombinant protein was purified through the 6×His tag by immobilized-metal ion affinity chromatography with EDTA-resistant Ni Sepharose excel resin (GE Healthcare) and loaded on a nickel-chelating column (GE Healthcare). Fractions containing N protein were dialyzed and collected. Because the expressed BCoV N protein also contains His, Trx, and S tag-coding sequences, the resulting molecular weight is estimated to be ~65 kDa. To obtain N protein without the His tag, the tag along with Trx and S tags was removed using PreScission protease (GE Healthcare). To purify His-tagged PABP, pET28aPABP, which contains the PABP gene (GenBank accession no. NM_002568), was transformed into *E. coli* BL21(DE3) pLysS cells and the following procedures were similar to those for expression of N protein described above.

EMSA and K_d. An *in vitro* transcription reaction for synthesizing ^{32}P-labeled RNA for electrophoretic mobility shift assay (EMSA) was carried out using T7 RNA polymerase and [α-^{32}P]ATP as specified by the manufacturer (Promega). To purify ^{32}P-labeled RNA, the synthesized ^{32}P-labeled RNA was separated on 6% sequencing gels, and passive elution was performed, followed by phenol-chloroform extraction. The ^{32}P-labeled RNA and N protein were added to a binding reaction mixture containing 20 mM HEPES (pH 7.5), 6 mM $MgCl_2$, 1.5 μM EGTA, 22.5 mM NaCl, 330 mM KCl, 36% glycerol, 3.6 mM dithiothreitol (DTT), 82.5 μg/ml of bovine serum albumin (BSA), and 36% glycerol and incubated for 15 min at 37°C with 1 U/ml of RNasin (Promega) (final concentrations for ^{32}P-labeled RNA and N protein were 1 nM and 5 nM, respectively). Reactions with unlabeled competitor at 1-, 10-, and 100-fold excesses and nonspecific yeast tRNA (0.1 mg/ml) were also performed in parallel. The RNA-protein complexes were resolved on a native polyacrylamide gel in TBE buffer (50 mM Tris, 45 mM boric acid, 0.5 mM EDTA) at a constant voltage at room temperature, dried, and analyzed by autoradiography. To determine the binding affinity, a fixed concentration of 0.2 nM ^{32}P-labeled RNA was titrated with protein (0, 14, 71, 143, 286, and 533 nM), and the bound RNA-protein complexes were separated from unbound RNA using an 8% polyacrylamide gel. Free and bound RNAs were quantitated and fit to the Hill equation: RNA bound $= b \times [P]n/(K_d{}^n + [P]^n)$, where b is the upper binding limit, $[P]$ is the protein concentration, n is the Hill coefficient, and K_d is the dissociation constant. GraphPad Prism was used. K_d was calculated based on at least three independent experiments.

UV cross-linking of RNA to N protein. HEK-293T cells were mock infected or infected with BCoV. After 16 h of infection, the ^{32}P-labeled 65-nt poly(A) tail was transfected using Lipofectamine 2000 (Thermo Fisher Scientific) according to the manufacturer's instructions, and at 2 h posttransfection, cells were washed with PBS. Cells were subjected to irradiation on ice for 5 min at 254 nm with ~4,000 μW/cm^2 using a Spectrolinker (XL-1000; Spectrolinker). Cell lysates were collected and treated with RNase mix containig10 mM Tris (pH 7.5), 400 U/ml of micrococcal nuclease, 1 mM $CaCl_2$, 1% aprotinin, 2 mg/ml of leupeptin-pepstatin, 100 mM phenylmethylsulfonyl fluoride (PMSF), and 0.1 mg/ml of RNase A and RNase T1) at 37°C for 30 min. RNase-treated samples were centrifuged, and supernatants were collected and precleared for 1 h at 4°C by incubation with protein G beads (MagQu). The beads were then removed and immunoprecipitated with an antibody against N protein at 4°C overnight, followed by incubation with protein G beads for 4 h at 4°C using tilt rotation. After extensive washing, the RNA-protein complexes were resuspended in SDS-PAGE loading dye, resolved by SDS-PAGE, dried, and visualized by autoradiography.

Immunoprecipitation and pulldown assay. His-tagged PABP (25 μg) was mixed with N protein in 100 μl of binding buffer containing 50 mM sodium phosphate (pH 7.4), 300 mM NaCl, and 0.02% Tween 20, and Qbeads-NTA-Ni (MagQu) were added. The mixture was incubated with tilt rotation for 30 min at room temperature. The beads were washed 3 times with 1 ml of binding buffer containing 50 mM sodium phosphate (pH 7.4), 300 mM NaCl, and 0.02% Tween 20. Proteins bound to the beads were eluted in SDS sample buffer, resolved by SDS-PAGE, and analyzed by Western blotting. The same method was employed to analyze proteins from cell lysates interacting with His-tagged N protein or His-tagged PABP in the presence or absence of RNase mix. Immunoprecipitation assay with N antibody bound to the protein G-coated magnetic beads followed by incubation with infected cell lysates was performed according to the manufacturer's instructions (MagQu). Proteins bound to the beads were analyzed by immunoblotting with antibody against eIF4G.

Biotinylated-RNA pulldown assays. To synthesize RNA labeled with biotin, the DNA template containing the 65-nt poly(A) tail and 19 non-poly(A) tail nucleotides or only 19 non-poly(A) tail nucleotides was used for *in vitro* transcription with T7 polymerase (Promega) in the presence of a biotin-UTP labeling nucleoside triphosphate (NTP) mixture (Roche), as recommended by the manufacturer. After purification, biotinylated RNA was incubated with cell lysates in Tris-EDTA (TE) buffer. After incubation at room temperature for 30 min, a streptavidin suspension (MagQu) was added to the mixture and incubated for 30 min at room temperature, followed by three washes with binding buffer. The protein-associated beads were boiled with SDS-PAGE loading buffer for 5 min and analyzed by immunoblotting.

***In vitro* and *in vivo* translation assays.** Capped transcripts for *in vitro* translation were prepared using a T7 mMessage mMachine kit (Ambion) according to the manufacturer's protocol. For the *in vitro* translation assay, 1 μg of capped transcript was added to a mixture containing 17.5 μl of rabbit reticulocyte lysate (RRL; Promega), 20 U of RNasin RNase inhibitor (Promega), 1 μl of amino acid mixture minus methionine, and 20 μCi of [^{35}S]methionine. After incubation at 30°C for 1 h, the samples were resolved by 10% SDS-PAGE. The gel was then dried and exposed to Kodak XAR-5 film. The films were

scanned and quantified with ImageJ software (NIH, Bethesda, MD). For a loading control, 1 μg of each capped transcript was resolved on a formaldehyde-agarose gel and stained with ethidium bromide, followed by band density quantitation using ImageJ software (NIH). For the effect of N protein on translation of DI-EGFP *in vivo*, HEK-293T cells were independently transfected with 3 μg of N protein or the His-tagged β-actin transcript using Lipofectamine 2000 (Thermo Fisher Scientific) according to the manufacturer's instruction. After 8 h of transfection, HEK-293T cells were transfected with 3 μg of DI-EGFP. Cell lysates were collected after 3, 8, and 16 h, and equivalent amounts of cell lysates were analyzed by immunoblotting. The amounts of translated products were normalized with loading control GAPDH and the amounts of DI-EGFP RNA quantified by RT-qPCR. For the effect of N protein on coronavirus translation *in vivo*, HEK-293T cells were independently transfected with 3 μg of N protein or the His-tagged β-actin transcript. After 8 h of transfection, HEK-293T cells were infected with BCoV. Cell lysates were collected at the time of postinfection as indicated in Fig. 4F, and equivalent amounts of cell lysates were analyzed by immunoblotting. The amounts of translated products were also normalized with loading control GAPDH and the amounts of BCoV genomic RNA quantified by RT-qPCR. For the effect of N protein on host protein synthesis, HEK-293T cells were mock transfected or independently transfected with N protein or the His–β-actin transcript. After 1 h, HEK-293T cells were incubated in medium in the presence or absence of actinomycin D (Thermo Fisher Scientific) for 8 h and incubated with methionine-free medium for 30 min followed by 20 μCi of [^{35}S]methionine for 1 h. The cells were then collected and equivalent amounts of cell lysates were analyzed by SDS-PAGE. The gel was exposed to X-ray film or Coomassie blue stained, followed by quantification with ImageJ software (NIH). The amounts of [^{35}S]methionine-labeled host proteins were then normalized with the amounts of Coomassie blue-stained proteins, and GAPDH mRNA was quantified by RT-qPCR.

Statistical analysis. Student's unpaired *t* test was used for statistical analysis of the data using Prism 6.0 software (GraphPad Software, Inc.). The values reported are presented as means ± standard deviations (SD) ($n = 3$).

ACKNOWLEDGMENTS

We thank Wei-Li Hsu at National Chung Hsing University, Taiwan, for assistance with the RNA-protein interaction experiment and Chih-Jung Kuo at National Chung Hsing University, Taiwan, for help with protein purification. We also dedicate this work to David A. Brian (1941-2014), University of Tennessee, and thank him for many helpful discussions in the initial stage of the work.

This work was supported by grants MOST 105-2320-B-005-004 and MOST 106-2313-B-005-046-MY3 from the Ministry of Science and Technology, Taiwan, Republic of China.

REFERENCES

1. King AMQ, Adams MJ, Carstens EB, Lefkowitz EJ (ed). 2011. Virus taxonomy. Classification and nomenclature of viruses. Ninth report of the International Committee on Taxonomy of Viruses. Elsevier Academic Press, San Diego, CA.
2. Lee S, Lee C. 2014. Complete genome characterization of Korean porcine deltacoronavirus strain KOR/KNU14-04/2014. Genome Announc 2:e01191-14. https://doi.org/10.1128/genomeA.01191-14.
3. Masters PS. 2006. The molecular biology of coronaviruses. Adv Virus Res 66:193–292. https://doi.org/10.1016/S0065-3527(06)66005-3.
4. Chen H, Gill A, Dove BK, Emmett SR, Kemp CF, Ritchie MA, Dee M, Hiscox JA. 2005. Mass spectroscopic characterization of the coronavirus infectious bronchitis virus nucleoprotein and elucidation of the role of phosphorylation in RNA binding by using surface plasmon resonance. J Virol 79:1164–1179. https://doi.org/10.1128/JVI.79.2.1164-1179.2005.
5. Nelson GW, Stohlman SA. 1993. Localization of the RNA-binding domain of mouse hepatitis virus nucleocapsid protein. J Gen Virol 74(Part 9): 1975–1979.
6. Cologna R, Spagnolo JF, Hogue BG. 2000. Identification of nucleocapsid binding sites within coronavirus-defective genomes. Virology 277: 235–249. https://doi.org/10.1006/viro.2000.0611.
7. Grossoehme NE, Li LC, Keane SC, Liu PH, Dann CE, Leibowitz JL, Giedroc DP. 2009. Coronavirus N protein N-terminal domain (NTD) specifically binds the transcriptional regulatory sequence (TRS) and melts TRS-cTRS RNA duplexes. J Mol Biol 394:544–557. https://doi.org/10.1016/j.jmb.2009.09.040.
8. Verheije MH, Hagemeijer MC, Ulasli M, Reggiori F, Rottier PJM, Masters PS, de Haan CAM. 2010. The coronavirus nucleocapsid protein is dynamically associated with the replication-transcription complexes. J Virol 84:11575–11579. https://doi.org/10.1128/JVI.00569-10.
9. Hurst KR, Ye R, Goebel SJ, Jayaraman P, Masters PS. 2010. An interaction between the nucleocapsid protein and a component of the replicase-transcriptase complex is crucial for the infectivity of coronavirus genomic RNA. J Virol 84:10276–10288. https://doi.org/10.1128/JVI.01287-10.
10. Hurst KR, Koetzner CA, Masters PS. 2013. Characterization of a critical interaction between the coronavirus nucleocapsid protein and nonstructural protein 3 of the viral replicase-transcriptase complex. J Virol 87:9159–9172. https://doi.org/10.1128/JVI.01275-13.
11. Denison MR, Spaan WJM, van der Meer Y, Gibson CA, Sims AC, Prentice E, Lu XT. 1999. The putative helicase of the coronavirus mouse hepatitis virus is processed from the replicase gene polyprotein and localizes in complexes that are active in viral RNA synthesis. J Virol 73:6862–6871.
12. Sims AC, Ostermann J, Denison MR. 2000. Mouse hepatitis virus replicase proteins associate with two distinct populations of intracellular membranes. J Virol 74:5647–5654. https://doi.org/10.1128/JVI.74.12.5647-5654.2000.
13. Stertz S, Reichelt M, Spiegel M, Kuri T, Martinez-Sobrido L, Garcia-Sastre A, Weber F, Kochs G. 2007. The intracellular sites of early replication and budding of SARS-coronavirus. Virology 361:304–315. https://doi.org/10.1016/j.virol.2006.11.027.
14. van der Meer Y, Snijder EJ, Dobbe JC, Schleich S, Denison MR, Spaan WJM, Locker JK. 1999. Localization of mouse hepatitis virus nonstructural proteins and RNA synthesis indicates a role for late endosomes in viral replication. J Virol 73:7641–7657.
15. Chang RY, Brian DA. 1996. cis requirement for N-specific protein sequence in bovine coronavirus defective interfering RNA replication. J Virol 70:2201–2207.
16. Yount B, Denison MR, Weiss SR, Baric RS. 2002. Systematic assembly of a full-length infectious cDNA of mouse hepatitis virus strain A59. J Virol 76:11065–11078. https://doi.org/10.1128/JVI.76.21.11065-11078.2002.
17. Almazán F, Galan C, Enjuanes L. 2004. The nucleoprotein is required for

efficient coronavirus genome replication. J Virol 78:12683–12688. https://doi.org/10.1128/JVI.78.22.12683-12688.2004.
18. Schelle B, Karl N, Ludewig B, Siddell SG, Thiel V. 2005. Selective replication of coronavirus genomes that express nucleocapsid protein. J Virol 79:6620–6630. https://doi.org/10.1128/JVI.79.11.6620-6630.2005.
19. Wu CH, Chen PJ, Yeh SH. 2014. Nucleocapsid phosphorylation and RNA helicase DDX1 recruitment enables coronavirus transition from discontinuous to continuous transcription. Cell Host Microbe 16:462–472. https://doi.org/10.1016/j.chom.2014.09.009.
20. Brockway SM, Clay CT, Lu XT, Denison MR. 2003. Characterization of the expression, intracellular localization, and replication complex association of the putative mouse hepatitis virus RNA-dependent RNA polymerase. J Virol 77:10515–10527. https://doi.org/10.1128/JVI.77.19.10515-10527.2003.
21. Miknis ZJ, Donaldson EF, Umland TC, Rimmer RA, Baric RS, Schultz LW. 2009. Severe acute respiratory syndrome coronavirus nsp9 dimerization is essential for efficient viral growth. J Virol 83:3007–3018. https://doi.org/10.1128/JVI.01505-08.
22. Züst R, Miller TB, Goebel SJ, Thiel V, Masters PS. 2008. Genetic interactions between an essential 3′ cis-acting RNA pseudoknot, replicase gene products, and the extreme 3′ end of the mouse coronavirus genome. J Virol 82:1214–1228. https://doi.org/10.1128/JVI.01690-07.
23. Deo RC, Bonanno JB, Sonenberg N, Burley SK. 1999. Recognition of polyadenylate RNA by the poly(A)-binding protein. Cell 98:835–845. https://doi.org/10.1016/S0092-8674(00)81517-2.
24. Gorgoni B, Gray NK. 2004. The roles of cytoplasmic poly(A)-binding proteins in regulating gene expression: a developmental perspective. Brief Funct Genomic Proteomic 3:125–141. https://doi.org/10.1093/bfgp/3.2.125.
25. Gingras AC, Raught B, Sonenberg N. 1999. eIF4 initiation factors: effectors of mRNA recruitment to ribosomes and regulators of translation. Annu Rev Biochem 68:913–963. https://doi.org/10.1146/annurev.biochem.68.1.913.
26. Merrick WC. 2004. Cap-dependent and cap-independent translation in eukaryotic systems. Gene 332:1–11. https://doi.org/10.1016/j.gene.2004.02.051.
27. Gamarnik AV, Andino R. 1998. Switch from translation to RNA replication in a positive-stranded RNA virus. Genes Dev 12:2293–2304. https://doi.org/10.1101/gad.12.15.2293.
28. Barton DJ, Morasco BJ, Flanegan JB. 1999. Translating ribosomes inhibit poliovirus negative-strand RNA synthesis. J Virol 73:10104–10112.
29. Yu IM, Gustafson CLT, Diao JB, Burgner JW, Li ZH, Zhang JQ, Chen J. 2005. Recombinant severe acute respiratory syndrome (SARS) coronavirus nucleocapsid protein forms a dimer through its C-terminal domain. J Biol Chem 280:23280–23286. https://doi.org/10.1074/jbc.M501015200.
30. Lo YS, Lin SY, Wang SM, Wang CT, Chiu YL, Huang TH, Hou MH. 2013. Oligomerization of the carboxyl terminal domain of the human coronavirus 229E nucleocapsid protein. FEBS Lett 587:120–127. https://doi.org/10.1016/j.febslet.2012.11.016.
31. Kühn U, Pieler T. 1996. Xenopus poly(A) binding protein: functional domains in RNA binding and protein-protein interaction. J Mol Biol 256:20–30. https://doi.org/10.1006/jmbi.1996.0065.
32. Knoops K, Kikkert M, van den Worm SHE, Zevenhoven-Dobbe JC, van der Meer Y, Koster AJ, Mommaas AM, Snijder EJ. 2008. SARS-coronavirus replication is supported by a reticulovesicular network of modified endoplasmic reticulum. PLoS Biol 6:1957–1974. https://doi.org/10.1371/journal.pbio.0060226.
33. Brown CG, Nixon KS, Senanayake SD, Brian DA. 2007. An RNA stem-loop within the bovine coronavirus nsp1 coding region is a cis-acting element in defective interfering RNA replication. J Virol 81:7716–7724. https://doi.org/10.1128/JVI.00549-07.
34. Chang RY, Hofmann MA, Sethna PB, Brian DA. 1994. A cis-acting function for the coronavirus leader in defective interfering RNA replication. J Virol 68:8223–8231.
35. Raman S, Brian DA. 2005. Stem-loop IV in the 5′ untranslated region is a cis-acting element in bovine coronavirus defective interfering RNA replication. J Virol 79:12434–12446. https://doi.org/10.1128/JVI.79.19.12434-12446.2005.
36. Spagnolo JF, Hogue BG. 2000. Host protein interactions with the 3′ end of bovine coronavirus RNA and the requirement of the poly(A) tail for coronavirus defective genome replication. J Virol 74:5053–5065. https://doi.org/10.1128/JVI.74.11.5053-5065.2000.
37. Wu HY, Brian DA. 2007. 5′-Proximal hot spot for an inducible positive-to-negative-strand template switch by coronavirus RNA-dependent RNA polymerase. J Virol 81:3206–3215. https://doi.org/10.1128/JVI.01817-06.
38. Soto Rifo R, Ricci EP, Decimo D, Moncorge O, Ohlmann T. 2007. Back to basics: the untreated rabbit reticulocyte lysate as a competitive system to recapitulate cap/poly(A) synergy and the selective advantage of IRES-driven translation. Nucleic Acids Res 35:e121. https://doi.org/10.1093/nar/gkm682.
39. Hong KY, Lee SH, Gu S, Kim E, An S, Kwon J, Lee JB, Jang SK. 2017. The bent conformation of poly(A)-binding protein induced by RNA-binding is required for its translational activation function. RNA Biol 14:370–377. https://doi.org/10.1080/15476286.2017.1280224.
40. Gross JD, Moerke NJ, von der Haar T, Lugovskoy AA, Sachs AB, McCarthy JE, Wagner G. 2003. Ribosome loading onto the mRNA cap is driven by conformational coupling between eIF4G and eIF4E. Cell 115:739–750. https://doi.org/10.1016/S0092-8674(03)00975-9.
41. Prevot D, Darlix JL, Ohlmann T. 2003. Conducting the initiation of protein synthesis: the role of eIF4G. Biol Cell 95:141–156. https://doi.org/10.1016/S0248-4900(03)00031-5.
42. Papadopoulos E, Jenni S, Kabha E, Takrouri KJ, Yi T, Salvi N, Luna RE, Gavathiotis E, Mahalingam P, Arthanari H, Rodriguez-Mias R, Yefidoff-Freedman R, Aktas BH, Chorev M, Halperin JA, Wagner G. 2014. Structure of the eukaryotic translation initiation factor eIF4E in complex with 4EGI-1 reveals an allosteric mechanism for dissociating eIF4G. Proc Natl Acad Sci U S A 111:E3187–E3195. https://doi.org/10.1073/pnas.1410250111.
43. Gingras AC, Raught B, Gygi SP, Niedzwiecka A, Miron M, Burley SK, Polakiewicz RD, Wyslouch-Cieszynska A, Aebersold R, Sonenberg N. 2001. Hierarchical phosphorylation of the translation inhibitor 4E-BP1. Genes Dev 15:2852–2864. https://doi.org/10.1101/gad.887201.
44. Wu HY, Brian DA. 2010. Subgenomic messenger RNA amplification in coronaviruses. Proc Natl Acad Sci U S A 107:12257–12262. https://doi.org/10.1073/pnas.1000378107.
45. Madhugiri R, Fricke M, Marz M, Ziebuhr J. 2016. Coronavirus cis-acting RNA elements. Adv Virus Res 96:127–163.
46. Wu HY, Ke TY, Liao WY, Chang NY. 2013. Regulation of coronaviral poly(A) tail length during infection. PLoS One 8:e70548. https://doi.org/10.1371/journal.pone.0070548.
47. Hofmann MA, Brian DA. 1991. The 5′ end of coronavirus minus-strand RNAs contains a short poly(U) tract. J Virol 65:6331–6333.
48. Bost AG, Prentice E, Denison MR. 2001. Mouse hepatitis virus replicase protein complexes are translocated to sites of M protein accumulation in the ERGIC at late times of infection. Virology 285:21–29. https://doi.org/10.1006/viro.2001.0932.
49. Lerner RS, Nicchitta CV. 2006. mRNA translation is compartmentalized to the endoplasmic reticulum following physiological inhibition of cap-dependent translation. RNA 12:775–789. https://doi.org/10.1261/rna.2318906.
50. King B, Brian DA. 1982. Bovine coronavirus structural proteins. J Virol 42:700–707.
51. Lapps W, Hogue BG, Brian DA. 1987. Sequence analysis of the bovine coronavirus nucleocapsid and matrix protein genes. Virology 157:47–57. https://doi.org/10.1016/0042-6822(87)90312-6.